



Deposited via The University of York.

White Rose Research Online URL for this paper:

<https://eprints.whiterose.ac.uk/id/eprint/207044/>

Version: Accepted Version

Article:

Yuan, Jing, Chen, Gaojie, Wen, Miaowen et al. (2023) Security-reliability tradeoff in UAV-carried active RIS-assisted cooperative networks. IEEE Communications Letters. ISSN: 1089-7798

<https://doi.org/10.1109/LCOMM.2023.3347294>

Reuse

This article is distributed under the terms of the Creative Commons Attribution (CC BY) licence. This licence allows you to distribute, remix, tweak, and build upon the work, even commercially, as long as you credit the authors for the original work. More information and the full terms of the licence here:

<https://creativecommons.org/licenses/>

Takedown

If you consider content in White Rose Research Online to be in breach of UK law, please notify us by emailing eprints@whiterose.ac.uk including the URL of the record and the reason for the withdrawal request.

Security-Reliability Tradeoff in UAV-Carried Active RIS-Assisted Cooperative Networks

Jing Yuan, Gaojie Chen, *Senior Member, IEEE*, Miaowen Wen, *Senior Member, IEEE*, Dehuan Wan, and Kanapathippillai Cumanan, *Senior Member, IEEE*

Abstract—In this letter, we propose an unmanned aerial vehicle (UAV)-carried active reconfigurable intelligent surface (RIS)-assisted cooperative network (UARC�N) with a source (S), a trustworthy user (U), and an untrustworthy user (E), which is bridged by multiple half-duplex decode-and-forward relays and an active RIS mounted on a hovering UAV. In the UARC�N, both U, E, and relays receive the signal from S through the active RIS merely in the first time slot; then one out of the successful decoding relays is selected to further transmit information via the direct link and RIS in the second time slot. The outage probability and intercept probability are jointly analyzed to investigate the security and reliability tradeoff (SRT) of the system. Simulation results validate our theoretical analysis, revealing that the active RIS can bring greater improvement to the system SRT than passive or hybrid RIS, and its location can be further optimized.

Index Terms—Active reconfigurable intelligent surface (RIS), relay, outage probability, intercept probability, security-reliability tradeoff.

I. INTRODUCTION

TO address the rising demands of data traffic, reliability, and security, the reconfigurable intelligent surface (RIS) has been proposed and thoroughly investigated over the past few years [1]. However, the widely known passive RIS-assisted systems have a double fading issue. Therefore, many researchers have combined relays with passive RIS to combat the double fading as well as harness the benefits of both. The authors of [2] utilized a decode-and-forward (DF) relay to improve the achievable rate of the system with only a weak link between the RIS and the destination. Besides, it has been demonstrated that the throughput of a RIS-relay-assisted cooperative system can be greatly improved by jointly

optimizing the relay selection and the reflection coefficients of RIS using deep reinforcement learning [3]. The authors of [4] proposed both the joint and integrated RIS and relay transmission schemes, and verified that the bit error rate and achievable rate are improved significantly compared to the single RIS networks. Moreover, several buffer-aided relays were used to enhance the RIS-assisted system in [5], and the authors maximized the secrecy rate with a delay constraint by jointly optimizing the relay selection and RIS coefficients.

However, the fixed position of the relay and RIS in [2]–[5] inevitably creates a problem: when the RIS is blocked by an obstacle and the performance improvement that the relay can bring to the system is weak, such a relay-RIS system will face a fatal blow. Therefore, some studies have investigated the complementarity of the unmanned aerial vehicle (UAV) and the RIS, which can provide more degrees of freedom to improve system performance. Specifically, the trace and transmit power of the UAV-mounted base station as well as the reflection coefficients of RIS installed on the facade of a building were jointly optimized to maximize the security rate in the presence of a legitimate user and an eavesdropper in [6], while the authors of [7] extended the work to a multi-user and multi-eavesdropper system and applied deep reinforcement learning to the similar optimization problem. In [8], the RIS was mounted on the UAV to connect the source and the user blocked by some obstacles, revealing significant improvements in the outage probability (OP) and bit error rate performance. Nevertheless, double fading still exists in the link associated with passive RIS in RIS-UAV cooperative networks. To further eliminate this negative effect, the active RIS, which can effectively resist the fading by amplifying the incident signal at the cost of energy consumption and noise, emerges recently. The authors of [9] analyzed the difference between active RIS and passive RIS from different perspectives and the performance differences brought by them. The safety of active RIS-assisted system was also discussed in [10]. However, there are few models of active RIS combined with UAVs and relays.

On the other hand, the above mentioned studies were either concerned with the reliability or security of the system, which, however, may interact with each other. For example, given a system comprising a legitimate user and an eavesdropper, if the OP of the legitimate link is reduced by increasing the transmit power, the risk of a successful interception on the wiretap link is also increased, and vice versa. Therefore, the authors of [11] proposed a relay selection system with the concept of security and reliability tradeoff (SRT) to strike a balance between system reliability and security, which are characterized by OP and intercept probability (IP), respectively. Since then, the SRT of extended networks, including the artificial noise-aided non-

Manuscript received August 20, 2023; revised November 28, 2023; accepted December 15, 2023. This work was supported in part by the Guangdong Basic and Applied Basic Research Foundation under Grant 2021B1515120067, in part by the National Natural Science Foundation of China under Grant 61971149, in part by the Guangdong Basic and Applied Basic Research Foundation under Grant 2021A1515011657, and in part by the UK Engineering and Physical Sciences Research Council (EPSRC) under grant number EP/X01309X/1. The associate editor coordinating the review of this letter and approving it for publication was H. Jung. (*Corresponding author: Gaojie Chen.*)

Jing Yuan is with the School of Information Engineering, East China Jiaotong University, Nanchang 330013, China (e-mail: jyuan59@163.com).

Gaojie Chen is with the 5GIC & 6GIC, Institute for Communication Systems, University of Surrey, Guildford, U.K., GU2 7XH. (e-mail: gaojie.chen@surrey.ac.uk).

Miaowen Wen is with the School of Electronic and Information Engineering, South China University of Technology, Guangzhou 510641, China (e-mail: eemwwen@scut.edu.cn).

Dehuan Wan is with Guangdong University of Finance, Guangzhou 510521, China (e-mail: wan_e@gduf.edu.cn).

Kanapathippillai Cumanan is with the School of Physics, Engineering and Technology, University of York, York, U.K., YO10 5DD. (email: kanapathippillai.cumanan@york.ac.uk).

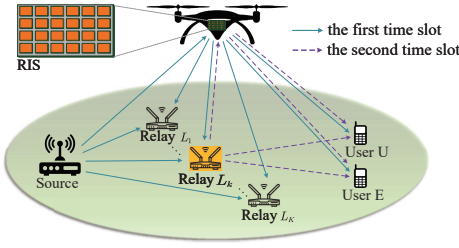


Fig. 1. The system model of UARCn.

orthogonal multiple access network, has been widely studied [12]. Motivated by the aforementioned, we investigate the SRT of a UAV-carried active RIS-assisted cooperative network (UARCn), where multiple half-duplex (HD) DF relays and a UAV-carried active RIS connect the source with the trustworthy and untrustworthy users. By dividing all possible cases into two main categories based on whether at least one HD DF relay successfully decodes the signal, we analyze the OP of the trustworthy link and IP of the untrustworthy link to jointly investigate the system SRT. Simulation results demonstrate the correctness of the theoretical analysis and show that, compared with the passive or the hybrid RIS strategy, the proposed active RIS method shows more potential to improve system SRT.

II. SYSTEM MODEL

The UARCn is shown in Fig. 1. Specifically, the system is composed of a source (S) and two receivers (the trustworthy user U and the untrustworthy user E), which are bridged by K HD DF relays¹. Let L_k denote the k th relay, where $k \in \mathbb{K} = \{1, 2, \dots, K\}$. Due to blockages, there are no direct links between S and U as well as between S and E. Therefore, a UAV-carried N -element active RIS (R) is used to enhance the network². Besides, all of S, U, E, and L_k , $k \in \mathbb{K}$ are equipped with a single antenna.

In the proposed system, S intends to send signal to U through the RIS and relays at a fixed data rate R_d over two time slots. Specifically, in the first time slot, a unit-power confidential signal $x \in \mathbb{C}$ is transmitted to U through the cascaded channel constructed by the RIS from S, and the multiple relays receive it at the same time. If all relays fail to decode the signal, they remain silent; otherwise, one of the successful decoding relays is selected to forward the signal to U through the cascaded and direct links in the second time slot. Meanwhile, the untrustworthy user E can wiretap the signals.

Without loss of generality, the path loss of all channel links is characterized by $\mathcal{L}_\Pi = C_0(d_\Pi/d_0)^{-\alpha_\Pi}$ with $\Pi = \{sr, sl_k, ru, re, rl_k, lk_r, lk_u, lke\}$ denoting the links S-R, S- L_k , R-U, R-E, R- L_k , L_k -R, L_k -U and L_k -E, $k \in \mathbb{K}$, where C_0 is the path loss at the reference distance $d_0 = 1$ m, and d_Π and α_Π denote the length and the path loss coefficient of the link Π , respectively. Let $h_{\Pi_1} = |h_{\Pi_1}|e^{j\varphi_{\Pi_1}} \in \mathbb{C}$, $\Pi_1 \in \{sl_k, lk_u, lke\}$ represent the channel coefficients of the link Π_1 which are

¹This model can be used in scenarios where some areas with existing relay equipment need to enhance communication in a short period of time.

²The optimization of UAV's trajectory can be achieved by the algorithms proposed in [6] and [7].

irrelevant to RIS, and $g_{\Pi_2} \in \mathbb{C}^N$, $\Pi_2 \in \{sr, rl_k, lk_r, ru, re\}$ denote those of the link Π_2 associated with the RIS with $g_{\Pi_2} = [|g_{\Pi_2}^1|e^{j\varphi_{\Pi_2}^1}, |g_{\Pi_2}^2|e^{j\varphi_{\Pi_2}^2}, \dots, |g_{\Pi_2}^N|e^{j\varphi_{\Pi_2}^N}]^T$. Therefore, it is natural to assume that h_{Π_1} follows $\mathcal{CN}(0, 1)$, and $g_{\Pi_2}^n$, $n \in \mathbb{N} = \{1, 2, \dots, N\}$ is modeled as normalized line-of-sight (LoS) link [6]. All channels are independent of each other and experience quasi-static flat fading over two time slots. The signals reflected by the RIS more than once are so weak that they can be ignored [1]. Moreover, E and U are assumed to belong to the same system, so we consider the statistical CSI for E [13].

Denote the amplitude and phase shift of the n th RIS element in the first time slot as a_n^\dagger and θ_n^\dagger , respectively, where \dagger represents the parameters in the first time slot. To maximize the received SNR of U, the phase shifts of RIS are set to the values that can offset the phase of the S-R-U link, namely $\theta_n^\dagger = -\varphi_{sr}^n - \varphi_{ru}^n$, $n \in \mathbb{N}$ [4]. Besides, for brevity, all elements are assumed to have the same amplitude, namely $a_n^\dagger = a_1$, $n \in \mathbb{N}$ with $a_1 > 1$ [14]. Therefore, the received SNRs of L_k , $k \in \mathbb{K}$, U and E in the first time slot can be expressed as

$$\begin{aligned} \gamma_{l_k}^\dagger &= \frac{P_s |\sqrt{\mathcal{L}_{sl_k}} h_{sl_k} + \sqrt{\mathcal{L}_{sr}\mathcal{L}_{rl_k}} a_1 \sum_{n=1}^N e^{j\vartheta_n^1}|^2}{\mathcal{L}_{rl_k} a_1^2 |\sum_{n=1}^N e^{j\vartheta_n^2}|^2 N_1 + N_0}, \\ \gamma_u^\dagger &= \frac{P_s \mathcal{L}_{sr} \mathcal{L}_{ru} a_1^2 N^2}{\mathcal{L}_{ru} a_1^2 |\sum_{n=1}^N e^{j\vartheta_n^3}|^2 N_1 + N_0}, \\ \gamma_e^\dagger &= \frac{P_s \mathcal{L}_{sr} \mathcal{L}_{re} a_1^2 |\sum_{n=1}^N e^{j\vartheta_n^4}|^2}{\mathcal{L}_{re} a_1^2 |\sum_{n=1}^N e^{j\vartheta_n^5}|^2 N_1 + N_0}, \end{aligned} \quad (1)$$

respectively, where $\vartheta_n^1 = \theta_n^\dagger + \varphi_{sr}^n + \varphi_{rl_k}^n$, $\vartheta_n^2 = \theta_n^\dagger + \varphi_{rl_k}^n$, $\vartheta_n^3 = \theta_n^\dagger + \varphi_{ru}^n$, $\vartheta_n^4 = \theta_n^\dagger + \varphi_{sr}^n + \varphi_{re}^n$, $\vartheta_n^5 = \theta_n^\dagger + \varphi_{re}^n$, P_s is the transmit power of S, and N_1 and N_0 denote the power of the noise at the elements of active RIS and the additive white Gaussian noise (AWGN) at the receiving nodes, respectively. Consequently, the capacities of S- L_k , $k \in \mathbb{K}$, S-R-U, and S-R-E links can be expressed as $C_{l_k}^\dagger = \frac{1}{2} \log_2(1 + \gamma_{l_k}^\dagger)$, $C_u^\dagger = \frac{1}{2} \log_2(1 + \gamma_u^\dagger)$, and $C_e^\dagger = \frac{1}{2} \log_2(1 + \gamma_e^\dagger)$, respectively.

Similarly, the amplitude and phase shift of the n th RIS element in the second time slot are denoted as a_n^\ddagger and θ_n^\ddagger , respectively, where \ddagger represents the parameters in the second time slot. The phase shifts of RIS are adjusted to align the signals from the cascaded channels with that from the direct link to maximize the received SNR of U, namely, $\theta_n^\ddagger = \varphi_{l_k u} - \varphi_{l_k r}^n - \varphi_{ru}^n$, and we assume that $a_n^\ddagger = a_2$, $n \in \mathbb{N}$ with $a_2 > 1$. Provided that at least one of the relays perfectly decodes the signal, there are 2^K possible sets containing all of the successful decoding relays, which is denoted as $\mathbb{L} \in \{\phi, \mathbb{L}_1, \mathbb{L}_2, \dots, \mathbb{L}_{2^K-1}\}$ with ϕ representing the empty set. When $\mathbb{L} \neq \phi$, the received SNRs of U and E from the selected relay $L_k \in \mathbb{L}$ in the second time slot can be expressed as

$$\begin{aligned} \gamma_{uk}^\ddagger &= \frac{P_l |\sqrt{\mathcal{L}_{l_k u}} h_{l_k u} + \sqrt{\mathcal{L}_{l_k r} \mathcal{L}_{ru}} a_2 N|^2}{\mathcal{L}_{ru} a_2^2 |\sum_{n=1}^N e^{j\vartheta_n^6}|^2 N_1 + N_0}, \\ \gamma_{ek}^\ddagger &= \frac{P_l |\sqrt{\mathcal{L}_{l_k e}} h_{l_k e} + \sqrt{\mathcal{L}_{l_k r} \mathcal{L}_{re}} a_2 \sum_{n=1}^N e^{j\vartheta_n^7}|^2}{\mathcal{L}_{re} a_2^2 |\sum_{n=1}^N e^{j\vartheta_n^8}|^2 N_1 + N_0}, \end{aligned} \quad (2)$$

respectively, where $\vartheta_n^6 = \theta_n^\dagger + \varphi_{ru}^n$, $\vartheta_n^7 = \theta_n^\dagger + \varphi_{lr}^n + \varphi_{re}^n$, $\vartheta_n^8 = \theta_n^\dagger + \varphi_{re}^n$, and P_l is the transmit power of the selected relay. Furthermore, instead of deriving the optimal relay with the help of an optimization method, we use a suboptimal solution here, that is, the selected relay from the successful decoding set is the one that maximizes the received SNR of U, which is expressed as³

$$L_* = \arg \max_{L_k \in \mathbb{L}, L_k \neq \phi} \gamma_{uk}^\dagger, \quad (3)$$

and the resulting SNRs of U and E in the second time slot can be denoted by γ_{u*}^\dagger and γ_{e*}^\dagger , respectively. Obviously, U and E can perform detection using both the received signal copies in the first and second time slots. Specifically, by using the selection combining (SC) rule, the achievable rates by U and E can be obtained by $C_u = \frac{1}{2} \log_2(1 + \max\{\gamma_u^\dagger, \gamma_{u*}^\dagger\})$ and $C_e = \frac{1}{2} \log_2(1 + \max\{\gamma_e^\dagger, \gamma_{e*}^\dagger\})$, respectively [11].

III. PERFORMANCE ANALYSIS

The OP of the trustworthy link and IP of the untrustworthy link are analyzed in this section. We note that $\vartheta_n^1 \sim \vartheta_n^8$, $n \in \mathbb{N}$ can be easily proved to be independent of each other and follow the uniform distribution in $[0, 2\pi)$.

A. The Analysis of OP

Considering the 2^K mutually exclusive possibilities of \mathbb{L} , the OP can be deduced as

$$P_{out} = \mathcal{P}(\mathbb{L} = \phi) \mathcal{P}(C_u^\dagger < R_d) + \sum_{i=1}^{2^K-1} \mathcal{P}(\mathbb{L} = \mathbb{L}_i) \mathcal{P}(C_u < R_d | \mathbb{L} = \mathbb{L}_i). \quad (4)$$

1) $\mathbb{L} = \phi$: No successful relay decoding means that the outage occurs in all the S- L_k , $k \in \mathbb{K}$ links in the first time slot, which can be expressed as

$$\mathcal{P}(\mathbb{L} = \phi) = \prod_{k=1}^K \mathcal{P}(C_{l_k}^\dagger < R_d) = \prod_{k=1}^K F_{\gamma_{l_k}^\dagger}(\Omega), \quad (5)$$

where $\Omega = 2^{2R_d} - 1$. Let $T_{1k} = \sqrt{\mathcal{L}_{slk}} h^{slk} + \sqrt{\mathcal{L}_{sr} \mathcal{L}_{rlk}} a_1 \sum_{n=1}^N e^{j\vartheta_n^1}$, and define the denominator of $\gamma_{l_k}^\dagger$ as T_{2k} . By applying the central limit theorem (CLT) and the rule for the sum of squares of Gaussian variables to the real and imaginary parts of T_{1k} , as well as by referring to [15] for T_{2k} , it can be deduced that the cumulative distribution function (CDF) of $\gamma_{l_k}^\dagger = P_s |T_{1k}|^2 / T_{2k}$ can be derived as

$$F_{\gamma_{l_k}^\dagger}(z) = 1 - \frac{\exp\left(\frac{-N_0 z}{P_s(\mathcal{L}_{slk} + N \mathcal{L}_{sr} \mathcal{L}_{rlk})}\right)}{1 + \frac{N \mathcal{L}_{rlk} a_1^2 N_1 z}{P_s(\mathcal{L}_{slk} + N \mathcal{L}_{sr} \mathcal{L}_{rlk})}}, \quad z \geq 0. \quad (6)$$

As a result, (5) is solved. On the other hand, we define $T_3 = |\sum_{n=1}^N e^{j\vartheta_n^3}|^2$ and we can infer that [15]

$$\mathcal{P}(C_u^\dagger < R_d) = \exp\left(-\frac{P_s \mathcal{L}_{sr} \mathcal{L}_{ru} a_1^2 N^2}{\mathcal{L}_{ru} a_1^2 N_1 N} - N_0\right). \quad (7)$$

³The performance analysis of the optimal relay situation will be studied in future work.

2) $\mathbb{L} = \mathbb{L}_i$, $i \in \{1, 2, \dots, 2^K - 1\}$: Afterwards, $\mathbb{L} = \mathbb{L}_i$ implies that all the received SNRs of the relays in \mathbb{L}_i satisfy the successful decoding requirement, while those of the others does not, which can be expressed as

$$\mathcal{P}(\mathbb{L} = \mathbb{L}_i) = \prod_{L_p \in \mathbb{L}_i} \left(1 - F_{\gamma_{l_p}^\dagger}(\Omega)\right) \prod_{L_q \notin \mathbb{L}_i} F_{\gamma_{l_q}^\dagger}(\Omega), \quad (8)$$

where $F_{\gamma_{l_k}^\dagger}(z)$ has been derived in (6). Thereafter, the OP based on \mathbb{L}_i over the two time slots is deduced as

$$\mathcal{P}(C_u < R_d | \mathbb{L} = \mathbb{L}_i) = \mathcal{P}(\gamma_u^\dagger < \Omega) \mathcal{P}(\gamma_{u*}^\dagger < \Omega | \mathbb{L} = \mathbb{L}_i), \quad (9)$$

where the first term on the right-hand side can be obtained in (7), while the second term is dependent on the selection of the optimal relay from \mathbb{L}_i . However, due to the randomness, every relay has the potential to be the best one. Therefore, according to the selection rule (3), the second term on the right-hand side can be expanded as

$$\begin{aligned} & \mathcal{P}(\gamma_{u*}^\dagger < \Omega | \mathbb{L} = \mathbb{L}_i) \\ &= \sum_{L_* \in \mathbb{L}_i} \mathcal{P}\left(\gamma_{u*}^\dagger \geq \max_{L_k \in \mathbb{L}_i, L_k \neq L_*} \gamma_{uk}^\dagger\right) \mathcal{P}(\gamma_{u*}^\dagger < \Omega). \end{aligned} \quad (10)$$

Define $T_{4k} = |\sqrt{\mathcal{L}_{l_k u}} h^{l_k u} + c_{4k}|^2$ and T_5 as the denominator of γ_{uk}^\dagger , where $c_{4k} = \sqrt{\mathcal{L}_{l_k r} \mathcal{L}_{ru}} a_2 N$. Referring to the Rayleigh distribution followed by $|h^{l_k u}|$ and the analysis of T_{2k} and $\gamma_{l_k}^\dagger$, the probability density function (PDF) of $\gamma_{uk}^\dagger / P_l = T_{4k} / T_5$ can be calculated to be

$$f_{\gamma_{uk}^\dagger / P_l}(z) \approx \sqrt{I_1 \mathcal{L}_{l_k u}} \exp\left(\frac{N_0 / I_1 - c_{4k}^2 / \mathcal{L}_{l_k u}}{8 I_1 \mathcal{L}_{l_k u} (\mathcal{L}_{l_k u} + I_1 z)^{7/2}}\right) \times (X_1 - X_2 - X_3 + X_4), \quad 0 \leq z \leq c_{4k}^2 / N_0, \quad (11)$$

where $I_1 = N \mathcal{L}_{ru} a_2^2 N_1$ and $X_1 \sim X_4$ are shown in (12) on the top of the next page. Consequently, the terms in (10) can be derived as

$$\mathcal{P}\left(\gamma_{u*}^\dagger \geq \max_{L_k \in \mathbb{L}_i, L_k \neq L_*} \gamma_{uk}^\dagger\right) = \prod_{L_k \in \mathbb{L}_i, L_k \neq L_*} \mathcal{P}\left(\frac{\gamma_{u*}^\dagger}{P_l} \geq \frac{\gamma_{uk}^\dagger}{P_l}\right)$$

$$\approx \prod_{L_k \in \mathbb{L}_i, L_k \neq L_*} \int_0^{\frac{c_{4k}^2}{N_0}} \int_0^u f_{\gamma_{u*}^\dagger / P_l}(u) f_{\gamma_{uk}^\dagger / P_l}(v) dv du, \quad (13)$$

$$\mathcal{P}(\gamma_{u*}^\dagger < \Omega) = \int_0^{\frac{\Omega}{P_l}} f_{\gamma_{u*}^\dagger / P_l}(z) dz, \quad (14)$$

where the approximation holds when assuming $\mathcal{L}_{l_p r} = \mathcal{L}_{l_q r}$, $p \neq q$, $p \in \{1, 2, \dots, K\}$, $q \in \{1, 2, \dots, K\}$ and (13) and (14) can be easily solved by mathematical softwares such as MATLAB through numerical integration. It should be noted that the later simulation results can also prove the feasibility of these approximations.

B. The Analysis of IP

Similarly, the IP can be derived as

$$P_{int} = \mathcal{P}(\mathbb{L} = \phi) \mathcal{P}(C_e^\dagger \geq R_d) + \sum_{i=1}^{2^K-1} \mathcal{P}(\mathbb{L} = \mathbb{L}_i) \mathcal{P}(C_e \geq R_d | \mathbb{L} = \mathbb{L}_i), \quad (15)$$

where $\mathcal{P}(\mathbb{L} = \phi)$ and $\mathcal{P}(\mathbb{L} = \mathbb{L}_i)$ are available in (5) and (8), respectively. It is not difficult to observe that both the

$$\begin{aligned}
 X_1 &= \exp\left(\frac{I_1 c_{4k}^2 z}{\mathcal{L}_{l_{ku}}(\mathcal{L}_{l_{ku}} + I_1 z)}\right) \sqrt{\pi z} \left(4I_1 c_{4k} (\mathcal{L}_{l_{ku}} + I_1 z) (2I_1 c_{4k}^2 z + \mathcal{L}_{l_{ku}}(\mathcal{L}_{l_{ku}} + I_1 z)) - 4I_1^2 c_{4k} z (2I_1 c_{4k}^2 z + 3\mathcal{L}_{l_{ku}}(\mathcal{L}_{l_{ku}} + I_1 z))\right) \\
 &\quad \times \left(\operatorname{erf}\left(c_{4k} \sqrt{\frac{I_1 z}{\mathcal{L}_{l_{ku}}(\mathcal{L}_{l_{ku}} + I_1 z)}}\right) + \operatorname{erf}\left(\frac{c_{4k} \mathcal{L}_{l_{ku}}}{\sqrt{I_1 \mathcal{L}_{l_{ku}}(\mathcal{L}_{l_{ku}} + I_1 z) z}}\right)\right), \\
 X_2 &= 4c_{4k} (\mathcal{L}_{l_{ku}} + I_1 z) \sqrt{z\pi} \exp\left(\frac{I_1 c_{4k}^2 z}{\mathcal{L}_{l_{ku}}(\mathcal{L}_{l_{ku}} + I_1 z)}\right) (2I_1^2 c_{4k}^2 z + I_1 \mathcal{L}_{l_{ku}}(\mathcal{L}_{l_{ku}} + I_1 z)) \left(1 + \operatorname{erf}\left(c_{4k} \sqrt{\frac{I_1 z}{\mathcal{L}_{l_{ku}}(\mathcal{L}_{l_{ku}} + I_1 z)}}\right)\right) \\
 &\quad + 8I_1 c_{4k}^2 (\mathcal{L}_{l_{ku}} + I_1 z) \sqrt{I_1 \mathcal{L}_{l_{ku}}(\mathcal{L}_{l_{ku}} + I_1 z) z}, \\
 X_3 &= 2z \sqrt{I_1 \mathcal{L}_{l_{ku}}(\mathcal{L}_{l_{ku}} + I_1 z)} \left((4I_1^2 c_{4k}^2 z + 4I_1 \mathcal{L}_{l_{ku}}(\mathcal{L}_{l_{ku}} + I_1 z)) \left(1 - \exp\left(\frac{c_{4k}^2 (I_1 z - \mathcal{L}_{l_{ku}})}{I_1 \mathcal{L}_{l_{ku}} z}\right)\right) - 4I_1 c_{4k}^2 (\mathcal{L}_{l_{ku}} + I_1 z) \right), \\
 X_4 &= \exp\left(\frac{I_1 c_{4k}^2 z}{\mathcal{L}_{l_{ku}}(\mathcal{L}_{l_{ku}} + I_1 z)}\right) \sqrt{\pi z} 4I_1^2 c_{4k} (2I_1 c_{4k}^2 z + 3\mathcal{L}_{l_{ku}}(\mathcal{L}_{l_{ku}} + I_1 z)) \left(1 + \operatorname{erf}\left(c_{4k} \sqrt{\frac{I_1 z}{\mathcal{L}_{l_{ku}}(\mathcal{L}_{l_{ku}} + I_1 z)}}\right)\right) \\
 &\quad + 8I_1^2 c_{4k}^2 z \sqrt{I_1 \mathcal{L}_{l_{ku}}(\mathcal{L}_{l_{ku}} + I_1 z)} + 8z (I_1 \mathcal{L}_{l_{ku}}(\mathcal{L}_{l_{ku}} + I_1 z))^{3/2}. \tag{12}
 \end{aligned}$$

numerator and denominator of γ_e^\dagger have the same construction as T_{2k} . Therefore, the CDF of γ_e^\dagger can be deduced to be

$$F_{\gamma_e^\dagger}(z) = 1 - \frac{\exp\left(\frac{-N_0 z}{N P_s \mathcal{L}_{sr} \mathcal{L}_{re}^2 a_1^4 N_1}\right)}{1 + \frac{\mathcal{L}_{re} a_1^2 N_1 z}{P_s \mathcal{L}_{sr} \mathcal{L}_{re} a_1^2}}, \quad z \geq 0. \tag{16}$$

Therefore, $\mathcal{P}(C_e^\dagger \geq R_d) = 1 - F_{\gamma_e^\dagger}(\Omega)$ is solved. Besides, the IP based on the decoding set and the optimal relay can be expanded as

$$\begin{aligned}
 \mathcal{P}(C_e \geq R_d | \mathbb{L} = \mathbb{L}_i) &= \\
 \sum_{L_* \in \mathbb{L}_i} \mathcal{P}\left(\gamma_{u_*}^\dagger \geq \max_{L_k \in \mathbb{L}_i, L_k \neq L_*} \gamma_{u_k}^\dagger\right) \mathcal{P}(\max\{\gamma_e^\dagger, \gamma_{e_*}^\dagger\} \geq \Omega), \tag{17}
 \end{aligned}$$

where the first term on the right-hand side can be found in (13). Then, the second term is equal to $1 - F_{\gamma_e^\dagger}(\Omega) \mathcal{P}(\gamma_{e_*}^\dagger < \Omega)$, where $F_{\gamma_e^\dagger}(\Omega)$ was solved in (16). Moreover, it is obvious that $\gamma_{e_*}^\dagger$ has the same structure as $\gamma_{l_k}^\dagger$. Therefore, it can be easily derived that

$$\mathcal{P}(\gamma_{e_*}^\dagger < \Omega) = 1 - \frac{\exp\left(-\frac{N_0 \Omega}{P_l (\mathcal{L}_{l_* e} + N \mathcal{L}_{l_* r} \mathcal{L}_{re} a_2^2)}\right)}{1 + \frac{N \mathcal{L}_{re} a_2^2 N_1 \Omega}{P_l (\mathcal{L}_{l_* e} + N \mathcal{L}_{l_* r} \mathcal{L}_{re} a_2^2)}}. \tag{18}$$

The proposed active RIS scheme is a generalized RIS-assisted design, which can degenerate into the passive RIS or hybrid RIS scheme by setting its parameters as follows: 1) when using a passive RIS, the value intervals of a_1 and a_2 become $[0, 1]$, and N_1 equals 0; 2) when using a hybrid RIS, only the corresponding parameters need to be adjusted according to the active or passive status of each element.

IV. SIMULATION RESULTS

In this section, simulation results are presented to validate the correctness of the theoretical analysis and explore the relationship between the SRT and other parameters. We consider a three-dimensional Cartesian coordinate system for the system model in Fig. 1 and uniformly define the coordinates of S, R, U, E, and the k th relay L_k , $k \in \mathbb{K}$ as $(\delta_{\Xi}^x, \delta_{\Xi}^y, \delta_{\Xi}^z)$, $\Xi \in \{s, r, u, e, k\}$. Unless otherwise specified, the parameters used in the following simulations are set as: the coordinates of all nodes are $\delta_s^x = -300$ m, $\delta_r^z = 200$ m, $\delta_u^x = \delta_e^x = 300$ m,

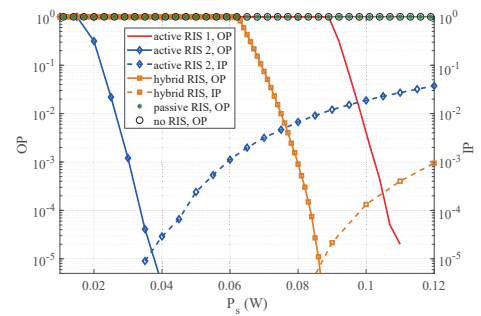


Fig. 2. OP and IP versus P_s with $P_l = 0.003$ W, $K = 3$, $N = 20$, and (1) active RIS 1: $a_1 = a_2 = 1.2$; (2) active RIS 2: $a_1 = a_2 = 2.7$; (3) hybrid RIS: half of the elements are active with $a_1 = a_2 = 1.2$, and the others are passive with $a_1 = a_2 = 1$; (4) passive RIS: $a_1 = a_2 = 1$.

$\delta_u^y = -50$ m, $\delta_e^y = 50$ m, $\delta_k^y = 10(k - K_0)$ m with $k \in \mathbb{K}$ and $K_0 = \lceil K/2 \rceil$ with $\lceil \cdot \rceil$ denoting the ceiling function, and the other coordinates equal 0; the path loss at the reference distance is $C_0 = 30$ dB; the path loss exponents of L_k -S, L_k -U, and L_k -E links are 2.8, 2.4, and 2.4 for $k \in \mathbb{K}$, respectively, and those of the other links are 2; both the power of the AWGN and that of the active RIS noise, namely N_0 and N_1 , equal -30 dB and -40 dB, respectively; the constant system data rate is $R_d = 1$ bps/Hz [11].

The OP and IP versus the transmit power of the source P_s are depicted in Fig. 2, which reveals the inhibition of OP and the enhancement of IP by increasing P_s , as well as the advantages of using the active RIS to improve the SRT in the considered cooperative network. It can be seen from the figure that, under the simulation condition, almost no interception occurs when there is no RIS, or a passive RIS, or an active RIS with the amplitudes of coefficients $a_1 = a_2 = 1.2$. However, for the first two cases, the OP is almost equal to 1, which makes the system impracticable, while the OP starts to drop rapidly in the active RIS case and hybrid RIS case where half of the elements are active. On the other hand, from the perspective of SRT, a good SRT (the intersection of the OP and IP curves is close to or less than 10^{-5}) can be achieved in the hybrid RIS case and both the two active RIS cases, while it cannot be obtained without RIS or with a passive RIS under the circumstance. Moreover, as seen from the location of the

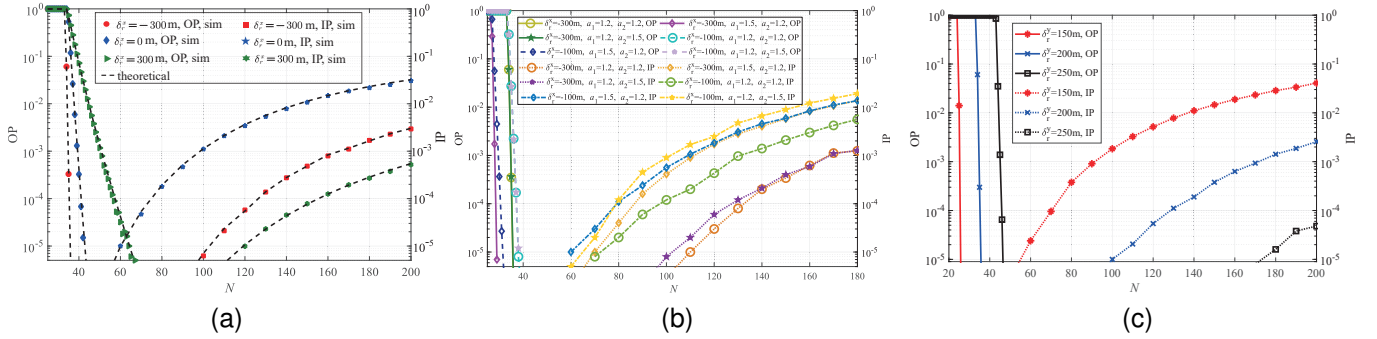


Fig. 3. Impact of (a) changing δ_r^x with $a_1 = a_2 = 1.2$ (b) changing a_1 and a_2 individually (c) changing δ_r^y with $a_1 = a_2 = 1.2$ on system SRT performance with $P_s = 0.03$ W, $P_l = 0.03$ W, and $K = 3$.

intersection points, the active RIS case requires less transmit power to obtain a good SRT than the hybrid RIS case.

Fig. 3 shows the relationships of OP, IP, and the coordinates of RIS. Firstly, in Fig. 3(a), three different RIS positions are considered, which are distinguished by the X-axis coordinates, and the simulation and theoretical curves of system OP and IP are depicted here. It is clear that the simulation and theoretical results are in high agreement, as well as that an increase of N inhibits the OP and augments the IP. Besides, when δ_r^x changes from -300 m to 0 m, the path loss on the S-R-U link becomes severe while those on the L_* -R-U/E links get conversely weaker. As a result, the OP is worse, whereas the IP becomes more threatening. The main reason is that, in the simulation condition, with the phase shift adjustment strategy of RIS, the SNR of U in the first time slot can already meet the data rate requirement, while that of E cannot. This is also confirmed in Fig. 3(b), where OP only changes with a_1 regardless of where RIS is, and as RIS moves closer to $\delta_r^x = 0$ m, IP is more affected by a_2 compared with a_1 . Furthermore, both the OP and IP get worse when δ_r^x varies from 0 m to 300 m, because this lethally affects the received SNRs of relays, resulting in a reduced probability of their successful decoding. Fig. 3(a) reveals that the optimal X-axis coordinate for RIS in the three cases is -300 m. Based on the above findings, we continue our exploration by changing the Z-axis coordinate when fixing δ_r^x at -300 m. As shown in Fig. 3(c), wherever the RIS is located, both the OP and IP can reach below 10^{-5} simultaneously, and the most proper location is $\delta_r^z = 150$ m. In conclusion, Fig. 3 reveals that a good SRT can always be obtained by using an active RIS wherever the RIS is, and the most economical approach is to place the RIS near the source to reduce the number of elements required.

V. CONCLUSION

This letter proposed a UARC� where a UAV-carried active RIS is utilized to strengthen the network consisting of a source and two users connected by multiple HD DF relays. The OP and IP of the system were analyzed, and simulations were carried out to discuss the influencing factors of the system SRT. Finally, simulation results confirmed the theoretical analysis and verified that active RIS improves the system SRT more than passive and hybrid RIS and it can be further improved by optimizing the location. In future work, we will continue

to discuss scenarios where perfect CSI for E can be obtained and will analyze the system SRT performance in more detail.

REFERENCES

- [1] Q. Wu, S. Zhang, B. Zheng, C. You, and R. Zhang, "Intelligent reflecting surface-aided wireless communications: A tutorial," *IEEE Trans. Commun.*, vol. 69, no. 5, pp. 3313–3351, May 2021.
- [2] Z. Abdullah, G. Chen, S. Lambotharan, and J. A. Chambers, "A hybrid relay and intelligent reflecting surface network and its ergodic performance analysis," *IEEE Wireless Commun. Lett.*, vol. 9, no. 10, pp. 1653–1657, Oct. 2020.
- [3] C. Huang, G. Chen, Y. Gong, M. Wen, and J. A. Chambers, "Deep reinforcement learning-based relay selection in intelligent reflecting surface assisted cooperative networks," *IEEE Wireless Commun. Lett.*, vol. 10, no. 5, pp. 1036–1040, May 2021.
- [4] I. Yildirim, F. Kilinc, E. Basar, and G. C. Alexandropoulos, "Hybrid RIS-empowered reflection and decode-and-forward relaying for coverage extension," *IEEE Commun. Lett.*, vol. 25, no. 5, pp. 1692–1696, May 2021.
- [5] C. Huang, G. Chen, and K.-K. Wong, "Multi-agent reinforcement learning-based buffer-aided relay selection in IRS-assisted secure cooperative networks," *IEEE Tran. Inf. Forensics and Secur.*, vol. 16, pp. 4101–4112, Aug. 2021.
- [6] S. Fang, G. Chen, and Y. Li, "Joint optimization for secure intelligent reflecting surface assisted UAV networks," *IEEE Wireless Commun. Lett.*, vol. 10, no. 2, pp. 276–280, Feb. 2021.
- [7] X. Guo, Y. Chen, and Y. Wang, "Learning-based robust and secure transmission for reconfigurable intelligent surface aided millimeter wave UAV communications," *IEEE Wireless Commun. Lett.*, vol. 10, no. 8, pp. 1795–1799, Aug. 2021.
- [8] L. Yang, P. Li, F. Meng, and S. Yu, "Performance analysis of RIS-assisted UAV communication systems," *IEEE Trans. Veh. Technol.*, vol. 71, no. 8, pp. 9078–9082, Aug. 2022.
- [9] Z. Zhang, L. Dai, X. Chen, C. Liu, F. Yang, R. Schober, and H. V. Poor, "Active RIS vs. passive RIS: Which will prevail in 6G?" *IEEE Trans. Commun.*, vol. 71, no. 3, pp. 1707–1725, Mar. 2023.
- [10] L. Dong, H.-M. Wang, and J. Bai, "Active reconfigurable intelligent surface aided secure transmission," *IEEE Trans. Veh. Technol.*, vol. 71, no. 2, pp. 2181–2186, Feb. 2022.
- [11] Y. Zou, X. Wang, W. Shen, and L. Hanzo, "Security versus reliability analysis of opportunistic relaying," *IEEE Trans. Veh. Technol.*, vol. 63, no. 6, pp. 2653–2661, Jul. 2014.
- [12] Z. Cao, X. Ji, J. Wang, W. Wang, K. Cumanan, Z. Ding, and O. A. Dobre, "Artificial noise aided secure communications for cooperative NOMA networks," *IEEE Trans. Cogn. Commun. Netw.*, vol. 8, no. 2, pp. 946–963, Jun. 2022.
- [13] L. Dong, H.-M. Wang, and H. Xiao, "Secure cognitive radio communication via intelligent reflecting surface," *IEEE Trans. Commun.*, vol. 69, no. 7, pp. 4678–4690, Jul. 2021.
- [14] Z. Yigit, E. Basar, M. Wen, and I. Altunbas, "Hybrid reflection modulation," *IEEE Trans. Wireless Commun.*, vol. 22, no. 6, pp. 4106–4116, Jun. 2023.
- [15] R. C. Ferreira, M. S. P. Facina, F. A. P. De Figueiredo, G. Fraidenraich, and E. R. De Lima, "Bit error probability for large intelligent surfaces under double-Nakagami fading channels," *IEEE Open J. Commun. Society*, vol. 1, pp. 750–759, May 2020.